

PROCEEDINGS OF SPIE

[SPIDigitalLibrary.org/conference-proceedings-of-spie](https://spiedigitallibrary.org/conference-proceedings-of-spie)

Corrosion monitoring along infrastructures using distributed fiber optic sensing

Alhandawi, Khalil, Vahdati, Nader, Shiryayev, Oleg, Lawand, Lydia

Khalil B. Alhandawi, Nader Vahdati, Oleg Shiryayev, Lydia Lawand, "Corrosion monitoring along infrastructures using distributed fiber optic sensing," Proc. SPIE 9803, Sensors and Smart Structures Technologies for Civil, Mechanical, and Aerospace Systems 2016, 980340 (20 April 2016); doi: 10.1117/12.2218820

SPIE.

Event: SPIE Smart Structures and Materials + Nondestructive Evaluation and Health Monitoring, 2016, Las Vegas, Nevada, United States

Corrosion monitoring along infrastructures using distributed fiber optic sensing

Khalil B. Alhandawi^a, Nader Vahdati^a, Oleg Shiryayev^a and Lydia Lawand^a

^aThe Petroleum Institute, Umm Al Nar, Main Campus, Dept. of Mechanical Engineering, Abu Dhabi, United Arab Emirates

ABSTRACT

Pipeline Inspection Gauges (PIGs) are used for internal corrosion inspection of oil pipelines every 3-5 years. However, between inspection intervals, rapid corrosion may occur, potentially resulting in major accidents. The motivation behind this research project was to develop a safe distributed corrosion sensor placed inside oil pipelines continuously monitoring corrosion. The intrinsically safe nature of light provided motivation for researching fiber optic sensors as a solution. The sensing fiber's cladding features polymer plastic that is chemically sensitive to hydrocarbons within crude oil mixtures. A layer of metal, used in the oil pipeline's construction, is deposited on the polymer cladding, which upon corrosion, exposes the cladding to surrounding hydrocarbons. The hydrocarbon's interaction with the cladding locally increases the cladding's refractive index in the radial direction. Light intensity of a traveling pulse is reduced due to local reduction in the modal capacity which is interrogated by Optical Time Domain Reflectometry. Backscattered light is captured in real-time while using time delay to resolve location, allowing real-time spatial monitoring of environmental internal corrosion within pipelines spanning large distances. Step index theoretical solutions were used to calculate the power loss due changes in the intensity profile. The power loss is translated into an attenuation coefficient characterizing the expected OTDR trace which was verified against similar experimental results from the literature. A laboratory scale experiment is being developed to assess the validity of the model and the practicality of the solution.

Keywords: Distributed sensing, Optical time domain reflectometry, Polymer clad silica fibers, Corrosion monitoring, Oil pipelines, Pipeline integrity management, Light Intensity field solutions, Multi-mode fibers

1. INTRODUCTION

Oil pipelines commonly used in the Oil and Gas industry are used as transfer lines spanning large distances. As part of the industry's efforts in ensuring asset integrity and employee welfare, a Pipeline Integrity Management (PIM) program was established at the Abu Dhabi National Oil Company (ADNOC) to assess and mitigate pipeline risks. In order to assess pipeline integrity a multitude of monitoring tools are developed. In the United Arab Emirates (UAE), the pipelines operate in weather conditions of extreme humidity and heat. As a result civil structures are frequently attacked by the various mechanisms of corrosion. Among the most widely used corrosion monitoring tools are the smart Pipeline Inspection Gauges (PIGs); a robotic probe propelled by the flow of oil that monitors the internal surface of the pipeline and performs thickness measurements of the pipeline's wall using Magnetic flux Leakage (MFL).¹ Other modern corrosion monitoring techniques include visual inspection probes employing Closed Circuit TV (CCTV) technology that enter pipelines to image the circumferential surface.² Another extensively used technique is via disposable corrosion coupons attached to the pipeline's walls and in contact with the internal environment.³ The corrosion current generated by the oxidation of iron is used to infer the corrosion rate.

All of the above methods share a common drawback which is responsible for production losses that occur during the act of inspection which is the requirement to invade the pipeline internally. Corrosion coupons on the other hand would require retrofitting of the existing pipelines in order to accommodate them which would also raise severe costs. Furthermore, crude oil mixture or petroleum products being transported are extremely

Further author information: (Send correspondence to Khalil B. Alhandawi)

Khalil B. Alhandawi: E-mail: khbalhandawi@pi.ac.ae, Telephone: +971 50 178 6051

Nader Vahdati: E-mail: nvahdati@pi.ac.ae, Telephone: +971 2 60 75787

Sensors and Smart Structures Technologies for Civil, Mechanical, and Aerospace Systems 2016,
edited by Jerome P. Lynch, Proc. of SPIE Vol. 9803, 980340 · © 2016 SPIE
CCC code: 0277-786X/16/\$18 · doi: 10.1117/12.2218820

volatile raising certain hazards with the use of electrical signals to communicate the conditions of the pipeline. As a result an intrinsically safe medium has been targeted to provide a solution that is economical and safe for pipeline environments using fiber optic sensing systems.

2. THEORETICAL BACKGROUND

In order to formulate an appropriate corrosion sensing solution to circumnavigate the drawbacks with existing conventional inspection tools, a review of the literature is required to study the existing techniques involving fiber optic sensors to measure corrosion directly or indirectly by exploiting various physical phenomena. A theoretical background on the desired sensing technique is then presented in order to develop a mathematical model which will be used as a design tool for the formulated solution.

2.1 Background on fiber optic sensors

An abundance of fiber optic sensors have been employed for local and distributed sensing applications for various physical phenomena.

Distributed sensing techniques for temperature measurements have been employed for leakage detection.⁴ Commercial systems have been developed that use Raman spectroscopy to obtain the spectral shift in a light pulse traveling through a fiber at multiple intervals along its length which are translated to temperature. Contact with the hot fluid from a leaky pipeline in vicinity of the fiber optic cable can help detect the fault early on. However, a proactive measure is required to characterize the corrosion rate and mitigate the problem beforehand. A similar technique that employs Optical Time Domain Reflectometry (OTDR) to interrogate the loss in light intensity due to chemical perturbations from a polymer clad fiber is described.⁵ When in contact with hydrocarbons, the refractive index (RI) of the polymer cladding is increased locally causing light intensity to be coupled out with the high order modes.⁵

The aforementioned methods were not specifically developed for corrosion sensing nor do they explicitly perform corrosion rate measurements. Other studies were performed employing stripped cladding fiber optic cables with metal coats on selected sections of the sensing fiber such that local corrosion causes the metal coat to erode directly exposing the core to the surroundings.⁶⁻⁸ When coated by a metal, traveling light incident on the metal layer is absorbed resulting in a power loss at the terminated end of the fiber. Upon corrosion, the metal is eroded exposing the core to the surrounding medium (air) resulting in the restoration of reflectivity which increases the detected power at the receiving end. Aluminum⁷ and carbon steel⁶ coatings were explored and both yielded similar results in terms of the progression of reflectivity in the presence of corrosion mechanisms.

In summary, a hybrid method utilizing OTDR detection techniques and the application of metal coatings from the parent structure will be utilized to formulate a true distributed corrosion sensing solution.

2.2 Theory and operation of OTDR diagnosis techniques

OTDR is a commonly used technique in the field of communication optics to diagnose fiber optic lines for imperfections and irregularities allowing spatial identification of faults. The technique employs a high power laser diode that fires a laser pulse through the fiber under inspection.⁹ As the pulse propagates through the fiber the signal is attenuated due to imperfections in the material and other inhomogeneities. An attenuation coefficient characterizes such losses and is usually specified by fiber optic cable manufacturers. As a result, power propagation through a fiber as a function of the distance traveled, z is given by the following relation:¹⁰

$$P(z) = P_0 10^{-\alpha z/10}, \quad (1)$$

where P_0 is the initial pulse power in W, α is the attenuation coefficient of the transmitting fiber in dBm^{-1} and z is the distance traveled in m. Equation (1) may be written in the \log_{10} form in order to assume the form of the equation of a line:

$$P_{dB}(z) = P_{0dB} - \alpha z, \quad (2)$$

where $P_{dB}(z) = 10 \log_{10} P(z)$. α gives the negative slope of the line. Any changes that cause an abrupt increase in the attenuation coefficient at a local position will cause a sudden increase in negative slope which is detected

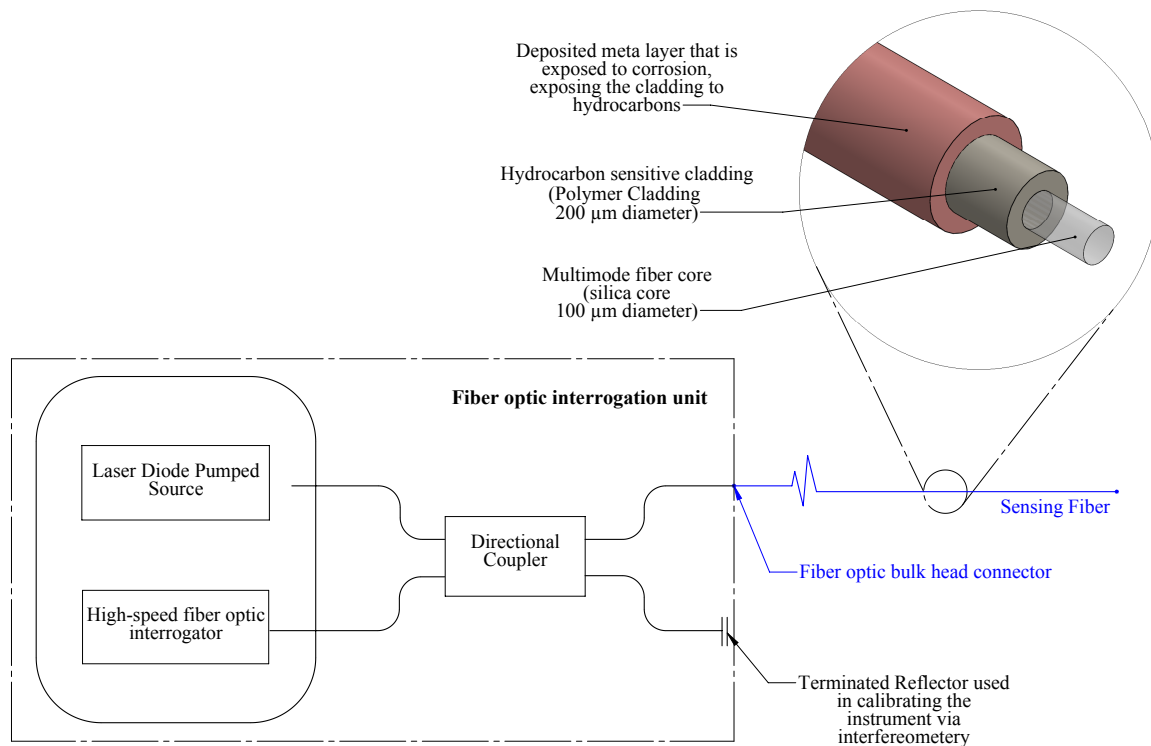


Figure 1: Schematic of distributed corrosion sensing fiber optic cable

by an OTDR interrogator that monitors the backscattered intensity; a fixed fraction of the total propagation intensity for a given transmission medium. In this study, by calculating the ratio of the transmitted intensity to the original total intensity, an attenuation coefficient for the perturbation interval is computed and is incorporated into Eqn. (2) to reflect the sudden change in slope.

3. METHODOLOGY AND SENSOR OPERATION PRINCIPLE

Based on the literature review from Sec. 2.1, a method that employs the coating techniques described by the literature in addition to the chemical sensing fibers employing polymer claddings was developed. The sensor layout is detailed in Fig. 1.

The operation principle of the proposed sensor relies on perturbation of the cladding by the surrounding hydrocarbons which occurs when the outer metal coating completely corrodes and exposes the cladding underneath. This problem will be modeled by utilizing the established theoretical models for light intensity distribution.

3.1 Analytical solutions to step-index profile problems

Step index fibers feature constant core and cladding RIs with a step drop to the cladding RI. An analytical solution exists for this type of fiber which is obtained by solving Maxwell's equations in conjecture with the wave equation for a cylindrical waveguide yielding the following well-known results:¹¹

$$e_{co}(r) = E_l \frac{J_l \left(V \sqrt{1-b} \frac{r}{a_{core}} \right)}{J_l (V \sqrt{1-b})} \quad (3)$$

$$e_{cl}(r) = E_l' \frac{K_l \left(V \sqrt{b} \frac{r}{a_{core}} \right)}{K_l (V \sqrt{b})}, \quad (4)$$

where J_l is the Bessel function of the first kind, K_l is the modified Bessel function of the second kind and E_l and E_l' are amplitude constants to be determined through boundary conditions. e_{co} and e_{cl} represent the radial intensity distributions for the core and cladding respectively and are to be solved for. The result of applying the continuity boundary condition at the core/cladding boundary yields the following results for the amplitude coefficients and the generalized guide index b :

$$E_l = E_l' \quad (5)$$

$$B a_{core} \frac{J_{l+1}(B a_{core})}{J_l(B a_{core})} = V^2 - (B a_{core})^2 \frac{K_{l+1} \left(V^2 - (B a_{core})^2 \right)}{K_l \left(V^2 - (B a_{core})^2 \right)}, \quad (6)$$

where $B = V / a_{core} \sqrt{1-b}$. The final result is substituted into cylindrical coordinates to yield the radial and azimuthal distributions:

$$\mathbf{e}_t(r, \phi) = e_{co}(r) \cos l\phi \hat{\mathbf{x}} \text{ for } r \leq a_{core}, \quad (7)$$

$$\mathbf{e}_t(r, \phi) = e_{cl}(r) \cos l\phi \hat{\mathbf{x}} \text{ for } r > a_{core}. \quad (8)$$

\mathbf{e}_t represents the cylindrical intensity distribution as a function of the radial and azimuthal coordinates used in cylindrical coordinates to define a circular fiber. They are obtained from the radial intensity distributions in Eqs. (3) and (4). l is the azimuthal mode number which can be any non-negative integer; 0, 1, 2,....

The established theoretical model will be used to compute the expected step-drop in an OTDR signal in a fiber characterized by Ref. 5 which conducted OTDR experiments on different hydrocarbons characterized by different RIs. The problem will be modeled as follows in the following section.

4. CHARACTERIZATION OF OTDR TRACES USING ESTABLISHED THEORETICAL MODELS

The experimental study carried out by Ref. 5 will be used to verify the model developed by calculating the step drop power loss following contact with certain hydrocarbon compounds. Table 1 summarizes the properties of the fiber optic cable used for the experimental setup in the subject article.

Table 1: Parameters characterizing the experimental waveguide fiber⁵ to verify solution methods

Parameter	Designation	Value
Core Radius (μm)	a_{core}	50
Cladding Outer Radius (μm)	b_{clad}	100
Core Refractive Index	n_{co}	1.456
Cladding Refractive Index	n_{cl}	1.436
Wavelength of Light Pulse (nm)	λ	850
Numerical Aperture	NA	0.24
Modal Capacity - V Number	V	88.89

A test was carried out assuming that the chemical in contact with the fiber was trichloromethane ($CHCl_3$) with a refractive index of 1.4459. The effect of mixing the optical properties of this particular hydrocarbon with the Polydimethylsiloxane (PDMS) polymer composing the cladding will be explored.

4.1 Refractive index perurbation mechanism

by assuming a mixed RI as a result of combining the optical properties of the hydrocarbon in question ($CHCl_3$) and the PDMS cladding by calculating the volume fraction of each constituent under the assumption of complete soaking of $CHCl_3$ into the PDMS cladding. The following outlines the calculations performed to obtain the volume fraction of the PDMS and $CHCl_3$ constituents in order to calculate the effective RI that results from the mixture of the two constituents.

Considering a unit volume of PDMS, the mass is given by: $m = V\rho$. A unit monomer is considered to have cylindrical dimensions: $V_m = \pi D_m^2 l_m / 4$. The number average molecular weight of a polymer molecule, i.e a polymer chain is $M_n = 117,962 \text{ g/mol}$ ¹² while the molecular weight of a polymer repeat unit $-[(CH_3)_2Si-O]_n-$ is $m_w = 74.154 \text{ g/mol}$ by summing the atomic mass of the constituent elements as reported in the periodic table. As a result the number of monomeric repeat units per chain is given by the degree of polymerization: $DP = M_n/m_w$. The mass of a single chain molecule is obtained using Avogadro's constant to convert from molecular weight to mass: $m_c = M_n/N_A$. The number of chains present in a unit volume of PDMS is $N_c = m_{total}/m_c = m_{total}N_A/M_n$. The product of the degree of polymerization and the volume of one repeat monomer unit results in the volume of a single polymer molecule or chain; $V_{polymer} = V_c N_c = V_m DP N_c = V_m M_n m_{total} N_A / m_w M_n = \rho V_{total} V_m N_A / m_w$. The volume fraction occupied by the polymer chains per unit volume is therefore given by the following: $V_{polymer}/V_{total} = \rho V_m N_A / m_w$. The remaining volume fraction is assumed to be that occupied by the hydrocarbon under the assumption of complete soaking of PDMS in $CHCl_3$, i.e all the free volume that is available is occupied by the hydrocarbon.

Table 2: Free volume calculation of PDMS polymer utilizing established PDMS properties

Parameter	Designation	Value
Number average molecular weight (g/mol) ¹²	M_n	73,474
Molecular weight of monomer repeat unit (g/mol)	m_w	74.154
Density of PDMS (kg/m^3) ¹³	ρ	970
Diameter of monomer repeat unit (\AA) ¹³	D_m	3.07
Length of monomer repeat unit (\AA) ¹³	l_m	2.69
Volume of monomer repeat unit (\AA^3)	$V_m = \pi D_m^2 l_m / 4$	19.91
Volume fraction of polymer to free volume (%)	$V_{polymer} = \rho V_m N_A / m_w$	15.60
Free volume fraction (%)	$1 - V_{polymer}$	84.40

In order to calculate the RI of a mixture of PDMS and $CHCl_3$ under the assumption that all the present free volume is occupied by the hydrocarbon, the generalized Lorentz-Lorenz relation¹⁴ is adapted for this problem:

$$\frac{n_{1 \rightarrow m}^2 - 1}{n_{1 \rightarrow m}^2 + 2} = \sum_{i=1}^m \phi_i \frac{n_i^2 - 1}{n_i^2 + 2}, \quad (9)$$

where $n_{1 \rightarrow m}$ is the RI of m constituents, n_i is the RI of each constituent and ϕ_i is the volume fraction of each constituent. Using the results from Table 2, the effective cladding refractive index is calculated as $n_{cl} = 1.44435$.

The results of the previous scenarios are summarized by Fig. 2 in order to depict the cases for which the light distribution is to be solved for.

4.2 Mode configuration in reference and perturbed fibers

Next, the corresponding permissible mode sets are computed in order to determine the number of modes propagating in the fiber and vary the parameters l and m in the theoretical equations used to obtain the intensity

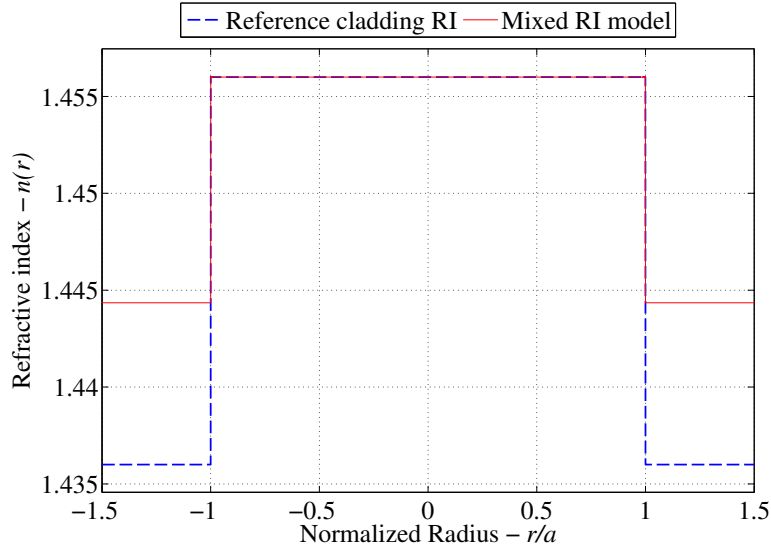


Figure 2: Possible refractive index profiles as a result of the soaking of PDMS clad fibers in $CHCl_3$

distribution for each individual mode. The mode sets are characterized by the following limiting equation for guided modes:¹⁰

$$l = 2(V/\pi - m) . \quad (10)$$

The limiting equation for leaky modes is given below. Leaky modes are radiated away after a cut-off distance from the launching end of the fiber due to the high attenuation associated with such modes:¹⁵

$$2m + l + 1 = M + l^2/4M , \quad (11)$$

Where $M = 2(V/\pi + 1)$.

Figure 3 represents the complete mode sets that are permitted by a reference fiber, Fig. 3a and the same fiber under a perturbation in the RI due to the saturation of the cladding by the hydrocarbon resulting in a higher mixed RI, Fig. 3b. Due to the assumption that the light pulse traveling down the fiber is developed before encountering a perturbation, leaky modes are exhibited and contributed to the light intensity only at the perturbed regions. Furthermore, since the perturbed sections of the fiber are typically smaller in length than the remainder of fiber, the leaky modes of the perturbed section are returned to the guided set of modes with the result that all other modes are permanently decoupled from the fiber. This effect is represented by the black hatched area in Fig. 3b. In other words, this area represents the lost energy from the fiber due to the perturbation.

Figure 3a represents the mode sets in a step index fiber, while Fig.3b represents the possible mode sets for the mixed RI approximation.

The previous approach determines which mode configuration should be solved for in order to calculate the difference in power levels between the reference fiber and the perturbed fiber such that their ratio is translated to an attenuation coefficient characterizing the step-drop height.

4.3 Cumulative light intensity distribution of all possible mode sets

Having developed an algorithm for determining the possible modes supported by the fiber, the solver is run for each mode while setting the amplitude constant E_l to unity. The intensity distribution \mathbf{e}_t is recorded and the corresponding power for each mode is calculated as:¹¹

$$P_{total} = \int_0^{2\pi} \int_0^\infty \frac{n}{\eta_0} \mathbf{e}_t^2 r dr d\phi . \quad (12)$$

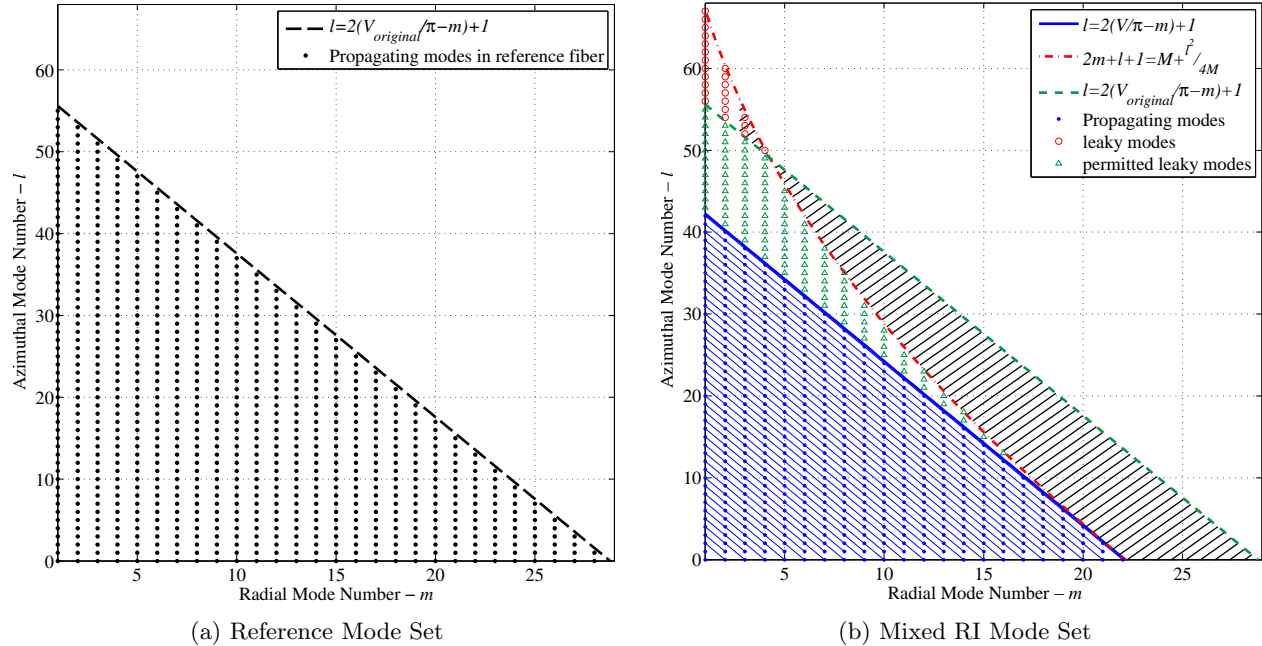


Figure 3: Permitted mode sets for (a) step index and diffusion modelled fibers and (b) mixed RI fibers

All the modes are normalized to carry unity power by dividing the square of each intensity distribution \mathbf{e}_l^2 by the total power carried as calculated in Eqn. (12) yielding the square of the normalized intensity distribution $\hat{\mathbf{e}}_l^2$. This manipulation ensures that all modes are equally excited in the fiber. The total power in the fiber is therefore given by the sum of all the normalized intensity distributions which will yield a total power equal to the number of modes excited since each mode carries unity power. The total power in the fiber may be controlled by setting the amplitude coefficient for all modes to be $E_l = P_{desired}/N_{modes}$, where N_{modes} is the number of modes.

However, the number of modes is not simply given by the number of permissible combinations of l and m as shown in Fig. 3. Examining Eqns. (7) and (8), for $l = 0$, it can be seen that the cosine terms become unity. However, for $l > 0$, the cosine terms may assume two identical states in terms of magnitude; $\cos(l\theta)$ and $\cos(l\theta + \pi/2)$ which results in each mode being counted twice due to the presence of two polarization states.¹⁵

By setting the power carried in each mode to an equal value in the case of the reference fiber and the perturbed fiber, solving for each mode and summing the normalized intensity distributions in order to obtain the net intensity distribution $\hat{\mathbf{E}}_{total}^2$, which is substituted into Eqn. (12) to obtain the total power supported by a fully filled fiber. The ratio of the power of the perturbed fiber to the reference is fiber is used to calculate the step drop per unit length (i.e the attenuation coefficient α) which characterizes the step drop:

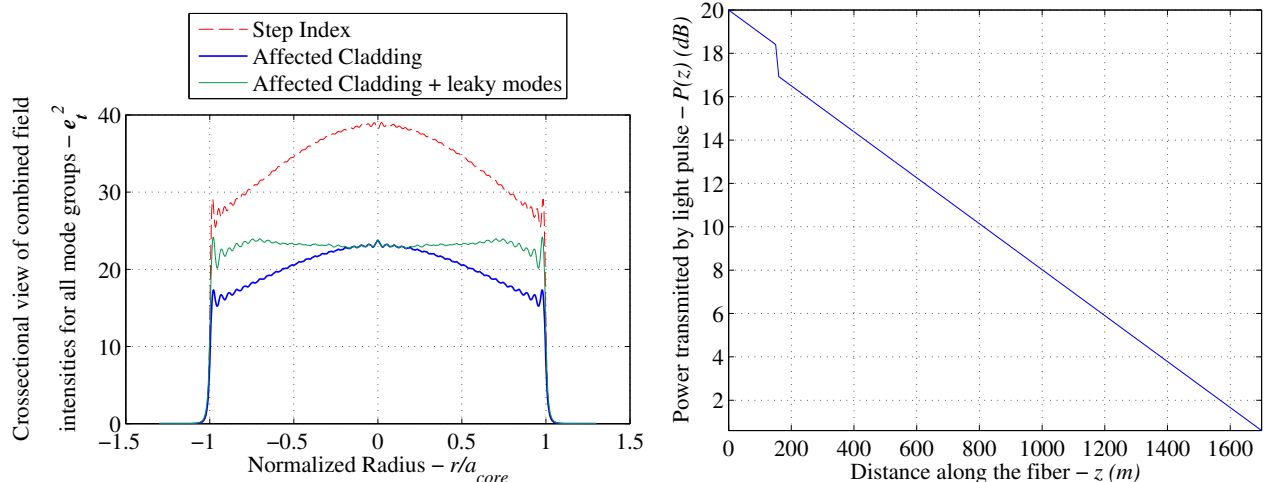
$$\frac{P_{perturbed}}{P_{reference}} = 10^{-\alpha\Delta z/10} ,$$

$$\alpha = -10 \log_{10} \left(\frac{P_{perturbed}}{P_{reference}} \right) / \Delta z , \quad (13)$$

Where Δz is the interval of the step drop usually set to a unit meter.

4.4 Power attenuation results for mixed refractive index fibers

Utilizing the pre-established mode sets in Fig. 3b, the analytical solution for step index fibers is used to obtain the light intensity solution for each mode and use the summation algorithm from Sec. 4.3 to obtain the cumulative light intensity distribution. The total results are reported in Fig. 4. The attenuation coefficient is then reported relative to the reference fiber and summarized in Sec. 4.5.



(a) Cumulative intensity of mixed RI and step index fibers

(b) Mixed RI attenuation trace

Figure 4: Simulation results for mixed RI fibers showing (a) the cumulative intensity distribution and (b) the expected attenuation (OTDR) trace for the calculated step drop

4.5 Verification of mixed refractive index fibers as models describing light intensity distributions in PDMS hydrocarbon systems

A comparison between the mixed RI fiber model and experiments in the literature is performed to determine how well the model captures the actual response of the sensor. Table 3 displays this result showing a comparable step drop in power levels.

Table 3: Comparison between the power transmission parameters for a reference fiber, a $CHCl_3$ saturated fiber and a mixed RI fiber

Parameter	Reference fiber	Mixed RI Fiber
Number of Supported Modes	1596	1162
Total guided power (mW)	100.016	72.9143
Power Loss (%)		27.10
Attenuation Coefficient (dBm^{-1})		1.373
Reported Attenuation Coefficient ⁵ (dBm^{-1})		1.46

Close agreement in the results between the reference experimental case and the mixed RI model is observed between the calculated step drop of 1.373 dBm^{-1} and the reported value of 1.46 dBm^{-1} . The discrepancy of 6.00% could be attributed to a number of reasons which will be discussed.

4.6 Discussion of experimental verification of theoretical mixed RI model

The calculated step drop displays a close agreement between the simulated data and the experimental data point obtained by.⁵ The discrepancy present can be attributed to missing chemical modeling required to obtain an accurate distribution of the RI profile throughout the cladding of the fiber when interacting with the hydrocarbon species in question. Furthermore, another contributing factor to such discrepancies may be due to the absorption coefficient of the hydrocarbon species which is likely to be contributed to that of the cladding.

Another possible cause for the observed discrepancy would be the incorporation of leaky modes into the total guided power after the perturbation is removed. The power contributed by the leaky modes may have already been radiated by the end of the perturbed section of the fiber. The assumption that this perturbed region is infinitesimal is not necessarily the case in the measurements of Ref. 5. According to,¹⁶ a leaky mode is defined as a mode that is attenuated to 1% of its original power value. This corresponds to a drop of 20 dB per meter according to Eqn. (13). If the perturbation length is assumed to be 1cm, then the drop would only be 0.2 dB

which is small enough but comparable to the calculated attenuation coefficient for $CHCl_3$ of around 1.373 dB from Table 3. Experimental studies for perturbations of varying length are required in order to accurately obtain the attenuation of each leaky mode and incorporate it into the net attenuation coefficient which would likely raise the calculated value to a value closer to the actual value.

Furthermore, the sensing band of the sensor must be estimated based on the developed model for applications in crude oil environments. Data obtained through material handbooks about the optical properties of several of these compounds¹⁷ revealed the need to redesign the sensing fiber based on the requirements of the operating environment. Alkanes being the main constituent of crude oil¹⁸ suggests that the sensing fiber's RI for the core and the cladding must span the region $1.3571 < n < 1.3886$ for the best response when in contact with crude oil.

Furthermore, based on the exact refractive index of the hydrophobic constituents which can be obtained through thorough laboratory tests, the RI of the cladding must be optimized such that an optimal step drop signal is achieved. The step drop must be large enough to be detected and should not lie at the lower band of the sensing range where sensitivity is minimal. The step drop signal must not be too large in order to allow the signal to be transmitted downstream of the perturbation without getting completely attenuated making further detection impossible.

5. CONCLUSION

A novel distributed sensor was studied and developed theoretically for the detection of internal corrosion within pipelines employing metal coated polymer-clad fiber optic cables. The theory suggests a good attenuation response to be observed when in contact with hydrocarbon compounds following failure of the metal coating. It was revealed that there are limitations on the sensing band of the fiber based on the optical properties of the environment it operates in. Furthermore, the presence of leaky modes following the start of a perturbation can be used to infer the length of the perturbation and therefore predict the volume of the coating corroded providing estimates of the corrosion rate. Experimental tests will be performed on the proposed setup to establish the above correlations while the results of the mixed RI model will be used to design the fiber for the experimental conditions that will be used to test the sensor's response.

ACKNOWLEDGMENTS

The authors are grateful to the Abu Dhabi National Oil Company (ADNOC) and the Abu Dhabi Company for Onshore Oil Operations (ADCO) for funding this research.

REFERENCES

- [1] Gloria, N. B., Areiza, M. C., Miranda, I. V., and Rebello, J. M., "Development of a magnetic sensor for detection and sizing of internal pipeline corrosion defects," *NDT&E International* **42**, 669–677 (June 2009).
- [2] Safizadeh, M. S. and Azzizadeh, T., "Corrosion detection of internal pipeline using NDT optical inspection system," *NDT&E International* **52**, 144–148 (Aug. 2012).
- [3] Ji, D. and Huang, Y., "Experimental study on seawater-pipeline internal corrosion monitoring system," *Sensors and Actuators B: Chemical* **135**, 375–380 (Sept. 2008).
- [4] Mirzaei, A., Bahrapour, A. R., Taraz, M., Bahrapour, A., Bahrapour, M. J., and Foroushani, S. A., "Transient response of buried oil pipelines fiber optic leak detector based on the distributed temperature measurement," *International Journal of Heat and Mass Transfer* **65**, 110–122 (June 2013).
- [5] Buerck, J., Roth, S., Kraemer, K., and Mathieu, H., "Otdr fiber-optical chemical sensor system for detection and location of hydrocarbon leakage," *Journal of Hazardous Materials* **102**, 13–28 (2003).
- [6] Saying, D., Yanbiao, L., Qia, T., Yanan, L., Zhigang, Q., and Shizhe, S., "Optical and electrochemical measurements for optical fibre corrosion sensing techniques," *Corrosion Science* **48**, 1746–1756 (2006).
- [7] Benounis, M. and Jaffrezic-Renault, N., "Elaboration of an optical fibre corrosion sensor for aircraft applications," *Sensors and Actuators B* **100**, 1–8 (Mar. 2004).
- [8] Cardenas-Valencia, A. M., Byrne, R. H., Calves, M., Langebrake, L., Fries, D. P., and Steimle, E. T., "Development of stripped-cladding optical fiber sensors for continuous monitoring II: Referencing method for spectral sensing of environmental corrosion," *Sensors and Actuators B* **122**, 410–418 (2007).

- [9] Udd, E. and Spillman, W. B., [*Fiber Optic Sensors: An Introduction for Engineers and Scientists, New Jersey: John Wiley & Sons, Inc.*] (1991).
- [10] Saleh, B. E. A. and Tiech, C. M., [*Fundamentals of Photonics, New Jersey: John Wiley & Sons*] (2007).
- [11] Chen, C. L., “2.3 generalized parameters,” in [*Foundation For Guided Wave Optics, Hoboken, New Jersey: John Wiley & Sons*], 25–50 (2007).
- [12] Wei, W., Xia, S., Liu, G., Dong, X., Jin, W., and Xu, N., “Effects of polydimethylsiloxane (PDMS) molecular weight on performance of PDMS/ceramic composite membranes,” *Journal of Membrane Science* **375**, 334–344 (2011).
- [13] Kuo, A., “Poly(dimethylsiloxane),” in [*Polymer Data Handbook, New York, Oxford University Press Inc.*], 411–435 (1998).
- [14] Plett, K. L., [*Development and Characterization of Polysiloxane Polymer Films for Use in Optical Sensor Technology*], PhD Thesis, Queens University, Kingston, Ontario, Canada (2008).
- [15] Hallam, A. G., [*Mode Control in Multimode Optical Fibre and its Applications*], M.S Thesis, Aston University, Photonics Research Group, Birmingham (2007).
- [16] Argyros, A. and Bassett, I. M., “Counting modes in optical fibres with leaky modes,” [*Online*]. Available: <http://sydney.edu.au/ipos/images/content/research/groups/mpof/SOFM.pdf>. [Accessed 20, Oct. 2015] .
- [17] Anderson, M. R., [*Determination of infrared optical constants for single components hydrocarbon fuels*], Master Thesis, University of Missouri-Rolla, USA (2000).
- [18] Jukic, A., “Petroleum refining and petrochemical processes; composition,” [*Online*]. Available: https://www.fkit.unizg.hr/_download/repository/PRPP_2013_Crude_oil_composition.pdf. [Accessed 20, Oct. 2015] .